

Universality and Deposition Morphology of Granular Column Collapses

Teng Man*

*Institute of Advanced Technology, Westlake Institute for Advanced Study,
18 Shilongshan Street, Hangzhou, Zhejiang 310024, China[†]*

Herbert E. Huppert

*Institute of Theoretical Geophysics, King's College, University of Cambridge,
King's Parade, Cambridge CB2 1ST, United Kingdom*

Ling Li and Sergio Andres Galindo-Torres[‡]

*School of Engineering, Westlake University, 18 Shilongshan Street,
Hangzhou, Zhejiang 310024, China*

(Dated: August 31, 2022)

Granular column collapses result in an array of flow phenomena and deposition morphologies, the understanding of which brings insights into studying granular flows in both natural and engineering systems. Guided by experiments, we carried out computational studies with the discrete element method (DEM) to identify fundamental links between the macro-scale behavior and micro-scale properties of granular columns. A physics-based non-dimensional number combining particle and bulk properties of the column, α_{eff} , was found to determinate three collapse regimes (quasi-static, inertial, and liquid-like), revealing universal trends of flow regimes and deposition morphologies under different conditions. This non-dimensional number represents physically the competing inertial and frictional effects that govern the behavior of the granular column collapse, including energy conversion and dissipation. The finding is important for understanding quantitatively the flow of granular materials and their deposits.

Usage: Secondary publications and information retrieval purposes.

Structure: You may use the `description` environment to structure your abstract; use the optional argument of the `\item` command to give the category of each item.

Granular materials are used widely and encountered frequently in a variety of areas of civil engineering, geophysics, pharmaceutical engineering, and chemical engineering[1, 2]. They can behave like a solid, a liquid, or a gas in different circumstances[3]. In recent decades, breakthroughs have been made to understand the basic governing principles, especially the constitutive relationships, of granular materials. Among these investigations, the proposal of the $\mu(I)$ rheology[4] and the $\mu(I, I_v)$ relationship[5, 6] of granular materials opened a window for exploring the behavior of dense granular materials from a viewpoint of a competition among acting stresses, viscous stresses and inertial stresses[5, 7] (or a competition among different time scales $1/\dot{\gamma}$, $d/\sqrt{\sigma_n/\rho_p}$, and η_f/σ_n [8], where $\dot{\gamma}$ is the shear rate, d the average particle radius, σ_n the pressure, ρ_p the particle density, and η_f the dynamic viscosity of the interstitial fluid).

The collapse of granular columns has drawn continuous attention due to the potential link to the dynamics and deposition morphologies of various geophysical flows[9, 10]. Progress has been made, even though no universal relationship describing the collapse of granular columns has been concluded. Difficulties arise because such systems are highly dependent on inter-particle friction[11] and boundary conditions[10, 12, 13], which were not fully captured by the rheological models previously mentioned. Some rigorous investigations[9, 14, 15] have been conducted to understand the behavior of granular column collapses. Lube et al.[9, 14] and Lajeunesse et al.[15] independently determined that relationships for both the normalized run-out distance $\mathcal{R} = (R_\infty - R_i)/R_i$ (where R_∞ is the final radius of the granular pile, and R_i the initial radius of the granular column), and the halt time of a collapsed granular column scale with the initial aspect ratio, $\alpha = H_i/R_i$ (where H_i is the initial height) of the column, a parameter drawn from dimensional analysis. Lube et al.[14] further concluded that inter-particle friction only plays an important role in the last instant of the flow when the collapse starts to halt. Staron and Hinch[11] studied the effect of grain properties on the collapse of granular columns and suggested that the frictional coefficient could have a significant impact on the run-out distance and final mass distribution. Kermani et al.[16] used the discrete element method (DEM) to investigate the relationship between deposition morphology and inter-particle rotational resistance as well as the initial porosity of the granular packing, based on which they linked the deposition morphology to the energy dissipation.

* manteng@westlake.edu.cn

† Also at School of Engineering, Westlake University

‡ s.torres@westlake.edu.cn

However, previous research often lacked physical interpretation of the scaling parameters, i.e. the initial aspect ratio α (which was derived from dimensional analysis[14]), and the universality of the transition point between the two determined relationships $\mathcal{R} \propto \alpha$ and $\mathcal{R} \propto \alpha^{1/2}$ [9, 14]. Furthermore, previous studies did not quantitatively take the inter-granular friction and boundary conditions into consideration. In this paper, with the assistance of both experiments and DEM simulations, we aim to explore further the scaling of the final run-out distance of collapsed granular columns and link the scaling law with a theoretically derived dimensionless number. The deposition morphology and the correlation between initial height and deposition distance are carefully analyzed. Three different collapsing types are observed and further associated with the ratio between inertial stresses and frictional stresses during granular column collapses. With this work, the regime transition of the granular column collapse can be obtained for further investigation of geophysical flows, such as debris flows and landslides.

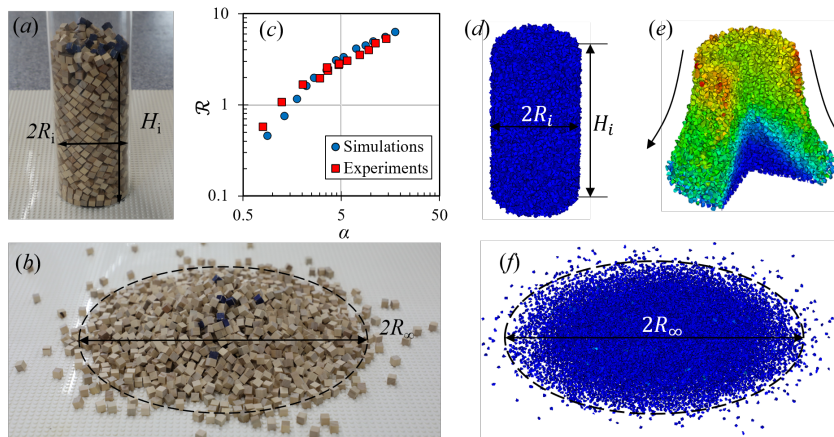


FIG. 1. (a) and (b) represent the experimental set-up and results of the collapse of dice; (c) shows the relationship between normalized run-out distance and the initial aspect ratio and the comparison between simulation and experimental results; (d - f) The initial, intermediate, and final DEM simulations of granular column collapse. The color in Fig. (d-f) represents the velocity field, especially in Fig. (e), different colors (from blue to red) show a spectrum of velocity magnitude from 0 cm/s to approximately 10 cm/s

In this study, we performed DEM simulations[17, 18] to test the collapse of granular columns, which allowed us to extract particle-scale data from the system. However, before diving deeply into the simulation setup, we first validated our DEM model with experiments. We performed experiments on the collapse of granular columns with wooden dice [Fig. 1(a) and (b)] of length 1.0 cm. The density of the dice was 0.681 g/cm^3 . They were dropped randomly into a circular tube ($D = 2R_i = 11.4 \text{ cm}$, where D is the internal diameter of the cross-section of the plastic tube, and R_i is the internal radius of the tube.). In the experiments, we used a LEGO board [Fig. 1(a)] as the bottom plate. The frictional coefficient between the board and the wooden dice was measured to be approximately 0.4, and the frictional coefficient between the wooden dice 0.84.

After placing the dice into the plastic tube [Fig. 1(a)], we measured the initial height of the granular packing, H_i . Then, the tube was manually lifted to release all the particles to form a granular pile. The run-out distance was measured as shown in Fig. 1(b). Thus, the relationship between \mathcal{R} and α was obtained [■ in Fig. 1(c)]. Because the tube was lifted manually, a disturbance would be applied to the granular pile while lifting, thus giving a relatively higher run-out distance when the initial aspect ratio is small.

We then performed numerical simulations with the same set-up as in the experiments of wooden dice [the DEM elements are cubic particles, as shown in Fig. 2(a)], to make sure our simulation set-up could capture the behavior of granular column collapses well. We varied the initial height of the granular column between 5 cm and 100 cm while keeping the initial cross-section diameter constant at 11.4 cm. In this set of simulations, we set the inter-particle frictional coefficient $\mu_p = 0.84$, particle/boundary frictional coefficient $\mu_w = 0.4$, and restitution coefficient $e = 0.2$. Blue markers in Fig. 1(c) show the results of this set of simulations. This shows that our model with a simple contact law represents the experimental data well, especially when the initial aspect ratio is large. When the initial aspect ratio is small, the experimental results tend to be larger than the simulation results. We believe this is due to the disturbance generated while manually lifting the tube during experiments.

Then, we performed simulations of the granular column collapses with Voronoi-based spheropolyhedra[18] [Fig. 1(d) - (f)]. The number of particles within unit length (1.0 cm) is 5, so the average particle size is $\approx 2 \text{ mm}$ [Fig. 2(b)]. Particles were packed within a column of radius R_i equal to 2.5 cm and varying heights H_i leading to cases of different initial aspect ratio α . Then, 20% of the Voronoi particles were removed to form a packing with a solid

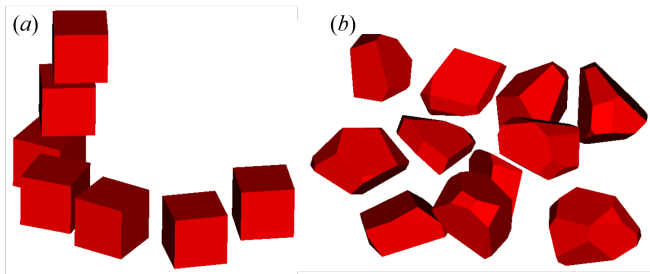


FIG. 2. (a) and (b) show cubic particles and Voronoi-based particles, respectively.

fraction of 0.8. We implemented a Hookean contact model (elaborated in the Method section below) with energy dissipation and restitution coefficient $e = 0.1$ to calculate the interactions between particles. A relatively low value of e was chosen to represent the rough surface of particles in real conditions[19]. Simulations were conducted with varied initial aspect ratios, α , between 0.4 and 20, varied inter-particle frictional coefficients, $\mu_p = 0.1, 0.2, 0.3, 0.4, 0.6, 0.8$, and particle/boundary frictional coefficients, $\mu_w = 0.2, 0.3, 0.4, 0.6, 0.8$. Based on these simulations we obtained the run-out behavior and deposition morphology for different conditions.

With either cubic or Voronoi-based spheropolyhedra (Fig. 2), we implement the Hookean contact model with an energy dissipation term to calculate the interactions among contacting particles[20]. At each time step, the overlap between adjacent particles, δ_n , is checked and the normal contact force can be calculated using

$$\vec{F}_n = K_n \delta_n \hat{n} - m_e \gamma_n \vec{v}_n, \quad (1)$$

where K_n is the normal stiffness characterizing the deformation of the material, \hat{n} is defined as the normal unit vector at the plane of contact, \vec{v}_n is the relative normal velocity between particles, m_e is the reduced mass of the particle pair, and γ_n is the normal energy dissipation constant, which depends on the coefficient of restitution e as [21, 22],

$$e = \exp \left(-\frac{\gamma_n}{2} \frac{\pi}{\sqrt{\frac{K_n}{m_e} - \left(\frac{\gamma_n}{2}\right)^2}} \right). \quad (2)$$

The tangential contact forces between contacting particles were calculated by keeping track of the tangential relative displacement $\vec{\xi} = \int \vec{v}_t dt$. Thus, the tangential contact forces follow

$$\vec{F}_t = -\min \left(|K_t \vec{\xi} + \gamma_t \dot{\vec{\xi}}|, \mu_p |\vec{F}_n| \right) \hat{t}, \quad (3)$$

where K_t is the tangential stiffness, $\dot{\vec{\xi}}$ is the rate of change of the tangential relative displacement, \hat{t} is the tangential vector in the contact plane and parallel to the tangential velocity, γ_t is the tangential energy dissipation constant, and μ_p is the frictional coefficient between contacting particles and can be replaced by the frictional coefficient between the particles and the bottom boundary, μ_w , while calculating the particle-boundary interactions. In this paper, we take $K_n = 1 \times 10^6$ N/cm, $K_t = 5 \times 10^5$ N/cm, and $\gamma_t = 0$ N-s/cm. The motion of particles is then calculated by step-wise resolution of Newton's second law with the normal and contact forces mentioned before.

In experiments, since the particles used were wooden dice, the collapse granular column could form a well-packed granular pile with an almost-circular boundary. We measured the diameters of the final pile along 4 different directions and took the average and divided it by 2 to obtain the final deposition radius. In simulations, the measurement of the final radius is more complicated than that in experiments. In cases with small particle-wall and particle-particle frictional coefficients but large initial aspect ratios, the spread of particles is far-reaching and leads to sparse (single layer) coverage of the area, especially at the front edge. In these cases, it is difficult to determine the edge/boundary and hence the final run-out distance. Thus, we measured the final radius with a histogram of particle distribution for each simulation. The following figure (Fig. 3) gives us two examples of how we measured the run-out distance.

In this figure, the x-axis is the radial position r , and the y-axis is the percentage of number of particles located within $(r - \Delta r/2, r + \Delta r/2)$ divided by the radial position, $P_{dm}(r) = (1/r)[N(r - \Delta r/2, r + \Delta r/2)/(\Sigma_r N)]$, where Δr is the bin width of the histogram, and $N(r - \Delta r/2, r + \Delta r/2)$ is the number of particles located between $r - \Delta r/2$ and $r + \Delta r/2$, and $\Sigma_r N$ is the total number of particles in one simulation. Fig. 3(a) shows the normalized particle number distribution (i.e. deposition morphology) of a simulation with $\mu_w = 0.2$, $\mu_p = 0.1$, and $H_i = 4$ cm. It shows that most particles locate within $r \leq 15$ cm; thus, we take $R_\infty = 15$ cm. Fig. 3(b) displays the particle

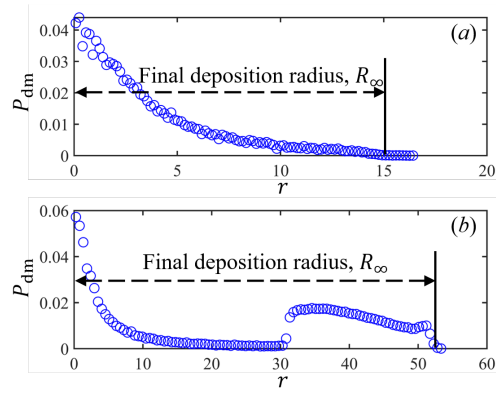


FIG. 3. Method for measuring the run-out distance of a collapsed granular column. (a) $H_i = 4$ cm, (b) $H_i = 40$ cm

distribution of a simulation with $\mu_w = 0.2$, $mu_p = 0.1$, and $H_i = 50$ cm. The results show that, besides particles located in the middle of the final granular pile, a large number of particles are located at the front, and when $r > 52$ cm, $(1/r)[N(r - \Delta r/2, r + \Delta r/2)/(\Sigma_r N)]$ became 0. Thus, the final radius of the collapsed granular column is 52 cm in this example.

Figure 4 shows relationships between normalized run-out distance \mathcal{R} and the initial aspect ratio α . It shows that both the inter-particle friction and the particle/boundary friction play important roles in the run-out behavior. Similar to results obtained by other research, when α is sufficiently small, \mathcal{R} scales roughly proportional to α ($\mathcal{R} \propto \alpha$). When α is larger than a threshold, \mathcal{R} scales approximately proportional to $\alpha^{1/2}$ ($\mathcal{R} \propto \alpha^{1/2}$).

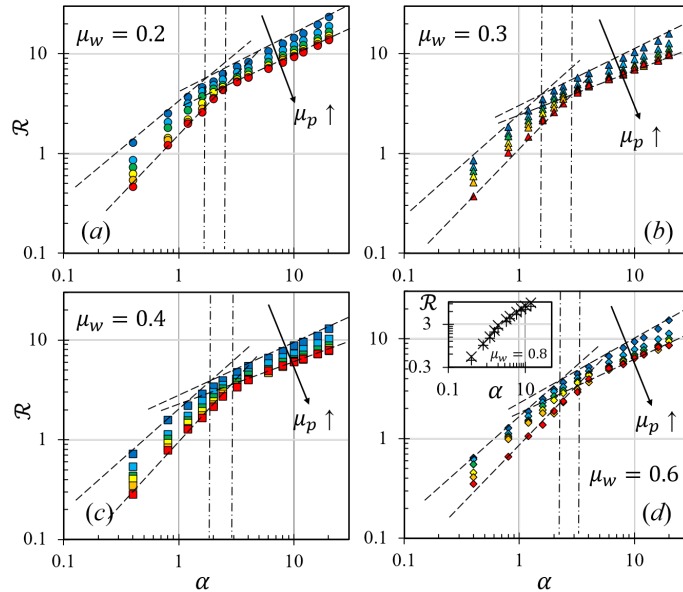


FIG. 4. (a) - (d) and the insert of Fig. (d) show the relationship between the normalized run-out distance, $\mathcal{R} = (R_\infty - R_i)/R_i$, and the initial aspect ratio, $\alpha = H_i/R_i$, with the particle/boundary frictional coefficient equal to 0.2 (circle markers), 0.3 (triangular markers), 0.4 (square markers), 0.6 (diamonds), 0.8 [\times for $\mu_p = 0.2$ and $+$ for $\mu_p = 0.4$ on the insert of Fig. (d)], respectively. Different color represents different inter-particle frictional coefficients. In Fig. (a), \bullet : $\mu_p = 0.1$, \circ : $\mu_p = 0.2$, \blacktriangle : $\mu_p = 0.3$, \square : $\mu_p = 0.4$, \circ : $\mu_p = 0.6$, \blacklozenge : $\mu_p = 0.8$. The dashed lines indicate the fitting power-law relations of cases with most frictional particles and least frictional particles in each sub-figure. The dash-dot lines show the transition points of cases with most frictional particles and least frictional particles in each sub-figure

In each of these figures, as we increase the inter-particle friction, the run-out distance decreases since the additional friction increases the energy dissipation during the collapse. Similar results can be obtained when we increase particle/boundary friction. Although qualitative observations have been witnessed by others, the quantitative influence of inter-particle and particle/boundary friction on the flowing behavior of collapsed granular columns has been absent

from previous studies. Also, as we vary the frictional coefficient, the point where the slope changes in the log-log plot of the $\mathcal{R} - \alpha$ relationship shifts, which indicates that the change of collapse regimes does not only depend on the α of the granular column.

To reveal the deposition morphology, we plot in Fig. 5(a)-(d) the deposition shapes of collapsed granular columns with different initial aspect ratios. We also distinguish particles initially located on the top of the column (blue dots) from the rest (red dots), while shading relatively stationary areas in yellow. The results show three different types of deposition morphology. When α is small [Fig. 5(a) and (b)], there is a plateau on top of the granular pile, and all blue dots present on top of red dots. In these cases, a large portion of particles remain stationary (yellow shaded area) during the collapse process, and the granular collapse behaves more like a yielded solid. Thus, we call it the quasi-static collapse. As we increase the initial aspect ratio [Fig. 5(c)], more particles flow down and spread out from the top of the column, and the inertial effect of particles starts to overtake the resistance of friction and become the dominating contribution. In these cases, top particles tend to rest at the foot of the final granular pile and during the collapse, surface granular flows (granular avalanches) dominate the behavior of the granular collapse. The final deposition morphology is similar to a typical sand pile. Thus, we name this type the inertial collapse, since inertial effects are dominating the macroscopic behavior. As we further increase α , the deposition surface changes to Fig. 5(d). Particles initially on the top end up being in the center of the final granular pile, indicating that during the granular collapse, the top particles are flowing downward while pushing the lower particles out, and the flow behaves more like a liquid. We call this type of granular collapse a liquid-like collapse.

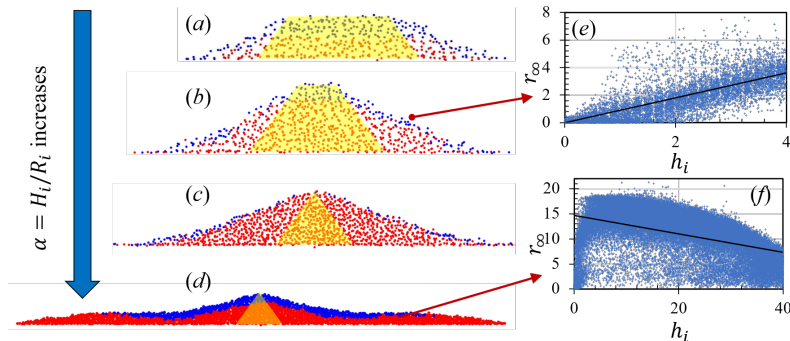


FIG. 5. (a) - (d) Deposition morphology of collapsed granular columns. Blue dots denote particles originally at the top 25% of the column, while red dots represent the rest. The yellow shaded areas roughly represent particles that remain stationary during collapses. (e) and (f) show the relationship between the initial height h_i and the final radial position r_i of each particle. The unit of the axes in (e) and (f) is centimeters

We can also see the transition in the plot of the relationship between the initial height h_i and the final radial position r_∞ of each particle [Fig. 5(e) and (f)]. When α is small [Fig. 5(e)], particles initially on the top tend to collapse to the front. Thus, the two parameters have a positive correlation. When α is large [Fig. 5(f)], particles initially on the top no longer reach the front of the final deposition. Thus, the two parameters have a negative correlation.

As we have stated, these three morphologies correspond to three collapsing regimes: (1) a quasi-static regime, where most bulk materials remain relatively stationary, and a plateau can form after the collapse; (2) an inertial regime, where particles initially at the top end up flowing to the front of the final pile; and (3) a liquid-like regime, where the collapsed granular materials flow like a liquid to form a much more complex morphology, where particles initially at lower height start to accumulate at the front of the flow due to the push-out effect from particles at higher initial heights.

Previous research argued that the run-out distance of a collapsed dry granular column is controlled almost entirely by the initial aspect ratio with little influence of friction. In contrast, we propose that the collapse and the deposition of a granular column is controlled by the ratio between inertial and frictional stresses. According to Bagnold [23, 24], in a dry granular flow, the inertial stresses scale with $\rho_p \dot{\gamma}^2 d^2$, where he took the distance between adjacent particles in the flowing (or shearing) direction as the characteristic length. We interpret $\dot{\gamma}$ as a rate change of unit deformation, and d as a length scale in the flowing direction. In our case, we simplify $\dot{\gamma}$ as $\sqrt{gH_i}/R_i$, which is the ratio between a characteristic velocity when particles fall over the length of H_i and the length scale, R_i , over which the deformation occurs. Meanwhile, d is replaced with H_i , giving the inertial stresses $\sigma_i = \rho_p (gH_i/R_i^2) H_i^2$. Additionally, the frictional stress can be calculated as $\sigma_f = \mu \sigma_n \propto \mu \phi_s \rho_p g H_i$, where ϕ_s is the solid fraction at the initial state. Thus the ratio between the two stresses can be obtained as

$$\frac{\sigma_i}{\sigma_f} \propto \frac{\rho_p (gH_i/R_i^2) H_i^2}{\mu \phi_s \rho_p g H_i} = \frac{1}{\mu \phi_s} \left(\frac{H_i}{R_i} \right)^2, \quad (4)$$

where μ is a general frictional coefficient, which we take as a linear combination of the inter-particle frictional coefficient and the particle-boundary frictional coefficient, $\mu = \mu_w + \beta\mu_b$, with β being a fitting parameter. The square root of this formula can be seen as an effective aspect ratio.

$$\alpha_{\text{eff}} = \sqrt{\frac{1}{(\mu_w + \beta\mu_b)\phi_s}} \left(\frac{H_i}{R_i} \right). \quad (5)$$

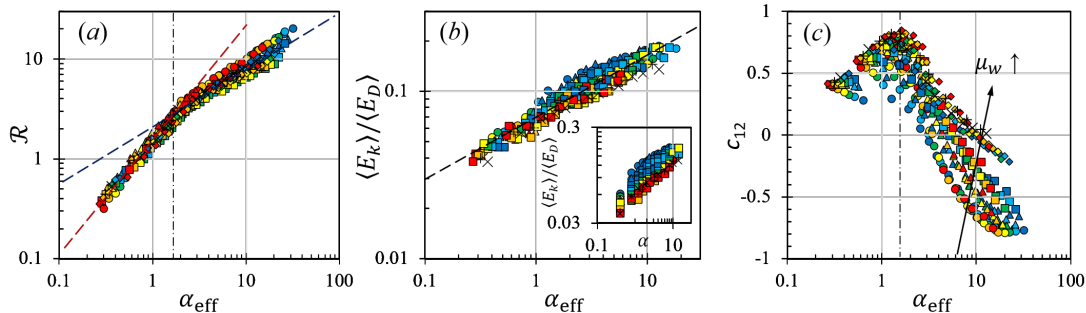


FIG. 6. (a) shows the relationship between \mathcal{R} and $\alpha_{\text{eff}} = (\sqrt{1/(\mu_w + \beta\mu_b)})(H_i/R_i)$. (b) presents $\langle E_k \rangle / \langle E_D \rangle$ against α_{eff} , where $\langle E_k \rangle$ is the time averaged kinetic energy generated during the granular collapse, and $\langle E_D \rangle$ is the time averaged dissipated energy. The inset of (b) plots $\langle E_k \rangle / \langle E_D \rangle$ against α in (c), the y -axis represents correlation coefficients between the initial height of particles and run-out distances of them, $c_{12} = \text{cov}[h_i, (r_\infty - r_i)] / (\sigma_h \sigma_r)$, where $\text{cov}[\]$ is the covariance function, and the x -axis shows α_{eff} . The markers have the same meaning as that in Fig. 4. The dashed lines in Fig. (a) and (b) are fitted power-law relations and the dash-dot lines in Fig. (a) and (c) indicate regime changes

In our simulations of the collapse of Voronoi granular columns, the initial solid fraction ϕ_s is the same for every case, so we leave ϕ_s out of our analyses, and $\beta = 2.0$ best fits the simulation data in Fig. 6(a) [the collapsed $\mathcal{R}(\alpha_{\text{eff}})$ relationship is not sensitive to $\beta \in (1.5, 5.0)$]. The parameter β can be roughly seen as a ratio between energy dissipated by inter-particle friction to that by particle/boundary friction. $\beta = 2.0$ indicates that the particle/boundary friction-induced energy dissipation plays a lesser role in the frictional energy dissipation. Fig. 6(a) shows the relationship between \mathcal{R} and α_{eff} . With $\beta = 2.0$, simulation results with different inter-particle friction and particle/boundary friction almost all collapse onto a single master curve, except when $\mu_w = 0.2$ and $\alpha_{\text{eff}} \gtrsim 3.0$. In contrast to previous studies, for which α is the only criterion to indicate a regime change [where the slope of $\mathcal{R}(\alpha)$ changes] and no influence of frictional coefficient was quantitatively considered, we find that, as depicted in Fig. 6(a), the slope change in the $\mathcal{R}(\alpha)$ relationship occurs at a unique value of α_{eff} for all cases. This indicates that \mathcal{R} is almost entirely controlled by α_{eff} , which includes the influence of both inter-particle and particle/boundary friction, rather than α alone. The reason why run-out distances for $\mu_w = 0.2$ deviate from other cases is that under low particle-boundary friction, granular columns tend to form only one layer of particles with few inter-particle contacts, thus increasing the scattering condition. In other cases, particles have a more resistant reaction with the boundary condition and adjacent particles, where the kinetic energy of particles can be quickly dissipated.

We also analyze the data from the viewpoint of energy consumption. For each simulation, we obtained the kinetic energy at time t , $E_k(t)$ and calculated the time averaged kinetic energy using $\langle E_k \rangle = (1/\tau) \int_0^\tau E_k(t) dt$, where τ is the terminating time of the granular column collapse. We then calculated the time averaged dissipated energy $\langle E_D \rangle = (1/\tau) \int_0^\tau [E_p(t) + E_k(t) - E_p(0)] dt$, where $E_p(t)$ is the potential energy of the system at time t and $E_p(0)$ is the initial potential energy. We plot the ratio between $\langle E_k \rangle$ and $\langle E_D \rangle$ with respect to α_{eff} in Fig. 6(b), which shows that $\langle E_k \rangle / \langle E_D \rangle$ has a power-law correlation with α_{eff} , whereas the data points fail to collapse onto a power-law relation when we use α as the x -axis [inset of Fig. 6(b)]. This indicates that the effective aspect ratio is linked not only to the ratio between inertial stresses and frictional stresses, but also to the energy consumption ratio during the collapse.

To analyze the influence of inter-particle friction and particle/boundary friction separately, in Fig. 7(a) we plot the relationship between the final coordination number, Z_c , and α_{eff} , where Z_c stands for the average number of inter-particle contacts one particle has inside a granular assembly. When $\mu_w = 0.4, 0.6, 0.8$, $Z_c \gtrsim 2.0$, which means that a cone-shape granular pile can be formed after the granular column collapse. However, when $\mu_w = 0.2$ and α_{eff} is large, Z_c is decreased to between 1.0 and 1.5, which indicates that most particles are scattered on the plane with almost no inter-particle contacts. This fits our assumption that, when μ_w is small, the influence of particle/boundary interactions should be larger than other cases, hence, $\beta = 2.0$ might be no longer valid.

We then studied the ratio of the contribution from particle-boundary friction and that from inter-particle friction, and then connected this ratio of contributions with the energy dissipated by those two kinds of frictions,

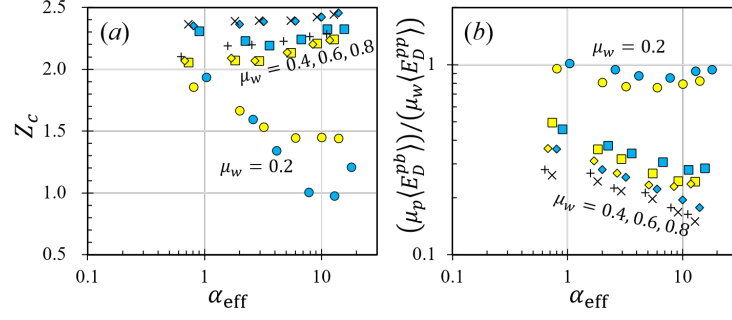


FIG. 7. (a) The relationship between coordination number, Z_c , and α_{eff} , where the coordination number, Z_c , stands for the average number of contacts a particle has in a granular assembly; (b) The relationship between $(\mu_p \langle E_D^{pb} \rangle) / (\mu_w \langle E_D^{pp} \rangle)$ and α_{eff} , where $\langle E_D^{pb} \rangle$ is the time average of the energy dissipated by particle-boundary frictions, and $\langle E_D^{pp} \rangle$ stands for the time average of the energy dissipated by particle-particle frictions.

$(\mu_w \sigma_n) / (\beta \mu_p \sigma_n) \sim \langle E_D^{pb} \rangle / \langle E_D^{pp} \rangle$, where $\langle E_D^{pb} \rangle$ is the time average of the energy dissipated by particle-boundary frictions, and $\langle E_D^{pp} \rangle$ stands for the time average of the energy dissipated by particle-particle frictions, so $(1/\beta) \sim [(\mu_p \langle E_D^{pb} \rangle) / (\mu_w \langle E_D^{pp} \rangle)]$. We plotted $(\mu_p \langle E_D^{pb} \rangle) / (\mu_w \langle E_D^{pp} \rangle)$ against α_{eff} in Fig. 7(b). For most cases, this ratio remains less than 0.5, while for cases with $\mu_w = 0.2$, this ratio is much larger, which fits our assumption that the contribution of particle-boundary friction exceeds our expectation and the energy dissipation from particle-boundary friction becomes the major dissipation source when the particle-boundary frictional coefficient is sufficiently small. This also implies that, when particle/boundary friction is small, $\beta = 2$ could not hold. More detailed analyses on particle-scale contact forces between particles and the boundary should be particularly investigated to verify this hypothesis in the future.

Figure 6(a) shows that the collapse of granular columns has two separate regimes based on the value of α_{eff} . However, according to the analysis of the deposition morphology, these granular flows should have three different regimes. To better investigate these regimes in connection to the deposition morphology, we analyze the relationship between the initial height, h_i , and the final radial position, r_∞ (or the run-out distance, $r_\infty - r_i$) of each particle. Such a relationship can help us better understand how particles end up being in different positions. The correlation coefficient between h_i and $r_\infty - r_i$ can then be obtained as

$$c_{12} = \frac{\text{cov}[h_i, (r_\infty - r_i)]}{\sigma_h \sigma_r}, \quad (6)$$

where c_{12} is the correlation coefficient between $r_\infty - r_i$ and h_i of particles in a collapsed granular column, $\text{cov}[\]$ is the covariance function[25], σ_h is the standard deviation of all the initial height data in one system, and σ_r is the standard deviation of all the run-out distances of particles in one system. When c_{12} is positive, more particles initially at the top of a granular column end up at the foot of the deposited pile, whereas when c_{12} is negative, more particles initially at the top cannot even reach the foot and more frequently end in the interior of the deposited granular packing, in which case, the collapse of granular columns behaves more like a fluid where top layer particles push the bottom layer particles away as they fall downward.

Figure 6(c) plots the relationship between c_{12} and α_{eff} . Both frictional coefficient and α_{eff} have great influence on how the c_{12} evolves. When α_{eff} is small, c_{12} is positive, and as we increase α_{eff} , c_{12} increases accordingly and eventually reaches a maximum, which corresponds to the turning point in the $\mathcal{R} - \alpha_{\text{eff}}$ relationship in Fig. 5(a). The α_{eff} value that corresponds to the maxima of c_{12} is a threshold which divides the quasi-static collapse and the inertial collapse. When α_{eff} is larger than this threshold, c_{12} starts to decrease, and, at a certain point, it becomes negative, where the collapse of a granular column is in the liquid-like regime.

However, the point when systems change from an inertial regime to a liquid-like regime depends not only on α_{eff} but also on other factors, as shown in Fig. 6(c), where the point of $c_{12}(\alpha_{\text{eff}})$ crossing the α_{eff} -axis is different for cases with different μ_w . Interestingly, if we plot c_{12} against $\alpha_{\text{eff}}/\mu_w$ instead [Fig. 8(a)], the place where c_{12} passes zero collapses onto one point, $\alpha_{\text{eff}}/\mu_w \approx 15$, which means that the transition from an inertial regime to a liquid-like regime depends on $\alpha_{\text{eff}}/\mu_w$. Based on these analyses, a phase diagram of the collapse of granular columns can be obtained as Fig. 8(b), where the collapse regime depends on both μ_w and α_{eff} . More specifically, the transition between quasi-static collapse and inertial collapse or liquid-like collapse depends only on the value of α_{eff} . In contrast, the transition between the inertial regime and the liquid-like regime depends on the ratio between α_{eff} and μ_w . It shows that the slope change in the $\mathcal{R}(\alpha_{\text{eff}})$ relationship (in log-log scale) corresponds to the regime change from quasi-static collapsing to the other

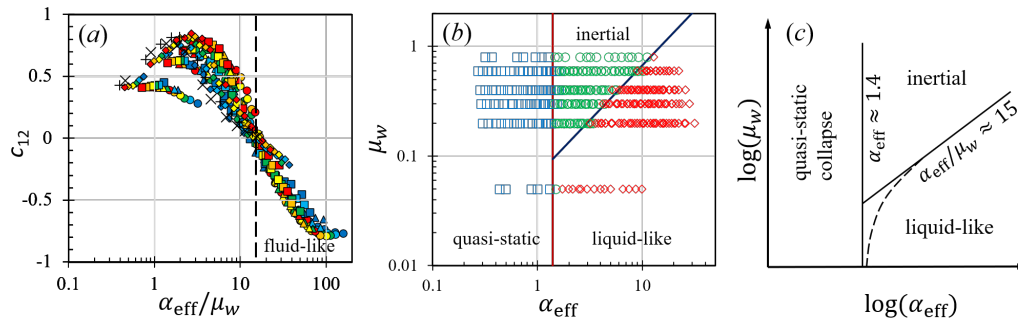


FIG. 8. (a) plots the relationship between c_{12} and $\alpha_{\text{eff}}/\mu_w$; (b) shows the transition among three collapse regimes. The solid lines in (b) indicate transition boundaries; (c) schematic diagram of the regime changes with respect to the effective aspect ratio α_{eff} and the boundary frictional coefficient μ_w . The dash line in (c) shows the possible transition from an inertial regime to a liquid-like regime

two regimes. This change is solely governed by the effective aspect ratio. Physically, it indicates that the inertial force needs to be above a certain threshold to overcome the frictional force (linear combination of the inter-particle friction and particle-boundary friction).

On the other hand, the change from an inertial collapse to a liquid-like collapse is mainly governed by $\alpha_{\text{eff}}/\mu_p$. When the granular column collapse is in a liquid-like regime, the curvature of the collapsed pile becomes non-monotonic and shows a more complex pattern. In this case, the initially top particles, instead of flowing to the front of the flow, end up flowing downward to push sub-layer particles to the front so that c_{12} becomes negative. It should be noted that we also performed simulations with $\mu_w = 0.05$, and expected a direct change from quasi-static collapsing to liquid-like collapsing. However, there is still one case showing granular column collapse in the inertial regime [Fig. 8(b)]. Thus, we suspect that when α_{eff} is approaching $\alpha_{\text{eff}} = 1.4$, the regime change between an inertial regime and a liquid-like regime should follow the dashed curve in Fig. 8(c). It should also be noted that since our definition of α_{eff} includes the packing solid fraction, it can be potentially useful in describing the behavior of granular column collapse with different initial packing fractions. Details of the influence of packing fraction will be further investigated in future publications.

In this paper, we analyzed the scaling of the run-out distance and deposition morphology of collapsed granular columns with respect to the aspect ratio based on numerical simulations. A physics-based dimensionless number α_{eff} , which is derived from the ratio between inertial stresses and friction-induced stresses and includes influences of the frictional coefficient (inter-particle and particle-boundary), the initial aspect ratio, and the initial solid fraction, is proposed. The α_{eff} can also be linked to the ratio between kinetic energy and collisionally dissipated energy. We showed that $\mathcal{R}-\alpha_{\text{eff}}$ relationships collapsed onto one curve for cases with different inter-particle and particle/boundary frictions. However, when $\mu_w = 0.2$ and α_{eff} is sufficiently large, the run-out distance is relatively larger than the prediction given by the mentioned collapsed curve. This is because when μ_w is small, particles tend to form a large area of one layer particles. During the formation of this one layer of particles, particle-boundary contacts dominate the sliding behavior of particles, while inter-particle contact becomes less frequent and less important.

Based on the correlation between the initial position and final position of particles, we further classify the collapse of granular columns into three regimes (quasi-static, inertial, and liquid-like), which are controlled by both α_{eff} and μ_w . This study shows that the boundary friction can be crucial to the final deposition of a collapsed granular column, which brings insight to the behavior of landslides or debris flows in future studies. The introduction of the solid fraction in α_{eff} , although it plays no role in this study, could bring opportunities to understand better in coming studies how the initial packing of granular materials influences the collapsing dynamics of granular materials in both sub-aerial and sub-aqueous environment. Additionally, the results of this paper have led us to further explore the intriguing collapsing behavior when the cross-section of the granular column is no longer axisymmetric. The different and exciting new results will be presented in another publication.

-
- [1] T. Man, *Rheology of Granular-Fluid Systems and Its Application in the Compaction of Asphalt Mixtures*, Ph.D. thesis, University of Minnesota (2019).
 [2] X. Zhang, Y. Wu, E. Zhai, and P. Ye, Coupling analysis of the heat-water dynamics and frozen depth in a seasonally frozen zone, *Journal of Hydrology*, 125603 (2020).

- [3] G. D. R. MiDi, On dense granular flows, *Euro Phys J E* **14**, 341 (2004).
- [4] P. Jop, Y. Forterre, and O. Pouliquen, A constitutive law for dense granular flows, *Nature* **441**, 727 (2006).
- [5] M. Trulsson, B. Andreotti, and P. Claudin, Transition from the viscous to inertial regime in dense suspensions, *Phys Rev Lett* **109**, 118305 (2012).
- [6] T. Man, Q. Feng, and K. M. Hill, Rheology of thickly-coated granular-fluid systems, arXiv preprint arXiv:1812.07083 (2018).
- [7] O. Pouliquen, C. Cassar, P. Jop, Y. Forterre, and M. Nicolas, Flow of dense granular material: towards simple constitutive laws, *J Stat Mech-Theory E* **2006**, P07020 (2006).
- [8] C. Cassar, M. Nicolas, and O. Pouliquen, Submarine granular flows down inclined planes, *Phys Fluids* **17**, 103301 (2005).
- [9] G. Lube, H. E. Huppert, R. S. J. Sparks, and A. Freundt, Collapses of two-dimensional granular columns, *Phys Rev E* **72**, 041301 (2005).
- [10] P.-Y. Lagr ee, L. Staron, and S. Popinet, The granular column collapse as a continuum: validity of a two-dimensional Navier–Stokes model with a μ (I)-rheology, *J Fluid Mech* **686**, 378 (2011).
- [11] L. Staron and E. Hinch, The spreading of a granular mass: role of grain properties and initial conditions, *Granul Matter* **9**, 205 (2007).
- [12] L. Staron and E. Hinch, Study of the collapse of granular columns using two-dimensional discrete-grain simulation, *J Fluid Mech* **545**, 1 (2005).
- [13] X. Zhang, K. Krabbenhoft, and D. Sheng, Particle finite element analysis of the granular column collapse problem, *Granul Matter* **16**, 609 (2014).
- [14] G. Lube, H. E. Huppert, R. S. J. Sparks, and M. A. Hallworth, Axisymmetric collapses of granular columns, *J Fluid Mech* **508**, 175 (2004).
- [15] E. Lajeunesse, J. Monnier, and G. Homsy, Granular slumping on a horizontal surface, *Phys Fluids* **17**, 103302 (2005).
- [16] E. Kermani, T. Qiu, and T. Li, Simulation of collapse of granular columns using the discrete element method, *Int J Geomech* **15**, 04015004 (2015).
- [17] P. A. Cundall and O. D. L. Strack, A discrete numerical model for granular assemblies, *Geotechnique* **29**, 47 (1979).
- [18] S. Galindo-Torres and D. Pedroso, Molecular dynamics simulations of complex-shaped particles using voronoi-based spheropolyhedra, *Phys Rev E* **81**, 061303 (2010).
- [19] X. Li, M. Dong, D. Jiang, S. Li, and Y. Shang, The effect of surface roughness on normal restitution coefficient, adhesion force and friction coefficient of the particle-wall collision, *Powder Technol* **362**, 17 (2020).
- [20] S. A. Galindo-Torres and D. M. Pedroso, Molecular dynamics simulations of complex-shaped particles using voronoi-based spheropolyhedra, *Phys Rev E* **81**, 061303 (2010).
- [21] F. Alonso-Marroqu n,  . Ram rez-G mez, C. Gonz lez-Montellano, N. Balaam, D. A. Hanaor, E. Flores-Johnson, Y. Gan, S. Chen, and L. Shen, Experimental and numerical determination of mechanical properties of polygonal wood particles and their flow analysis in silos, *Granul Matter* **15**, 811 (2013).
- [22] S. Galindo-Torres, X. Zhang, and K. Krabbenhoft, Micromechanics of liquefaction in granular materials, *Phys Rev Appl* **10**, 064017 (2018).
- [23] R. A. Bagnold, Experiments on a gravity-free dispersion of large solid spheres in a newtonian fluid under shear, *P Roy Soc Lond A Mat* **225**, 49 (1954).
- [24] K. M. Hill and B. Yohannes, Rheology of dense granular mixtures: Boundary pressures, *Phys Rev Lett* **106**, 058302 (2011).
- [25] D. M. Frangopol, Probability concepts in engineering: emphasis on applications to civil and environmental engineering (2008).